Adv. Manuf.
https://doi.org/10.1007/s40436-024-00523-y

The effect of the slope angle and the magnetic field on the surface quality of nickel-based superalloys in blasting erosion arc machining

Lin Gu[1,2] · Ke-Lin Li[1,2] · Xiao-Ka Wang[1,2] · Guo-Jian He[1,2]

Received: 28 March 2024 / Revised: 10 May 2024 / Accepted: 26 July 2024

Abstract Electrical arc machining (EAM) is an efficient process for machining difficult-to-cut materials. However, limited research has been conducted on sloped surface machining within this context, constraining the further application for complex components. This study conducts bevel machining experiments, pointing out that the surface quality becomes unsatisfactory with the increasing bevel angle. The discharge condition is counted and analyzed, while the flow field and the removed particle movement of the discharge gap are simulated, demonstrating the primary factor contributing to the degradation of surface quality, namely the loss of flushing. This weakens both the plasma control effect and debris evacuation, leading to the poor discharge condition. To address this issue, the magnetic field is implemented in blasting erosion arc machining (BEAM). The application of a magnetic field effectively regulates the arc plasma, enhances debris expulsion, and significantly improves the discharge conditions, resulting in a smoother and more uniform sloped surface with a reduced recast layer thickness. This approach provides the possibility of applying BEAM to complex parts made of difficult-to-cut materials in aerospace and military industries.

Keywords Blasting erosion arc machining (BEAM) · Surface quality · Machining angle · Magnetic field assisted

✉ Lin Gu
lgu@sjtu.edu.cn

✉ Ke-Lin Li
lkl19980123@sjtu.edu.cn

[1] State Key Laboratory of Mechanical System and Vibration, Shanghai Jiao Tong University, Shanghai 200240, People's Republic of China

[2] School of Mechanical Engineering, Shanghai Jiao Tong University, Shanghai 200240, People's Republic of China

1 Introduction

In order to improve the performance of aerospace parts, more and more types of materials with high-temperature mechanical properties are widely applied, such as nickel-based superalloys, metal matrix composites, and intermetallic alloys [1]. However, conventional methods are difficult to process these materials due to their high hardness and strength, causing long time and high costs. To overcome this issue, electrical arc machining (EAM) was proposed and utilized as a highly efficient technique for the removal of electro-conductive materials [2], particularly those that were challenging to cut. Compared to traditional cutting processes, EAM offers several advantages, including a significantly higher material removal rate (MRR) and lower costs. Within the realm of arc-based machining, researchers have proposed various methods, including arc dimensional machining (ADM) [3], high-speed electro erosion milling [4], blasting erosion arc machining (BEAM) [5], electrochemical arc machining [6], and electrical discharge and arc compound machining [7]. These techniques have found applications in the manufacturing of aerospace components such as bladed blisks [4] and turbine disks [8].

The surface machined by EAM is composed of overlapping craters, directly affecting the surface quality. Deep erosion craters are prone to be produced under the unsatisfactory discharge conditions such as long term stable arc and short circuit, resulting in uneven surfaces. The surface processed by negative polarity BEAM has a surface roughness R_a of 274 μm [9]. During short electrical arc machining (SEAM) of Inconel 718 using graphite electrodes, the surface roughness S_a increases with increasing voltage, and when the voltage is 30 V, S_a reaches 112.21 μm [10]. Therefore, the surface quality processed after EAM is frequently inferior and with the potential to improve. One

Published online: 11 September 2024

of the critical factors in enhancing the surface quality is effectively controlling the arc plasma during machining.

In EAM, to timely drive away or even break the stable arc, two arc breaking mechanisms, namely the mechanical motion arc breaking mechanism and hydrodynamic arc breaking mechanism, have been employed to effectively move the arc plasma [11]. However, when only relying on mechanical motion arc breaking mechanism [12], limitations in MRR and high tool wear ratio (TWR) were observed. This is due to the fact that high-speed gap flushing not only drives the arc plasma but also facilitates the expulsion of molten metal [13]. Some researchers have enhanced the hydrodynamic arc breaking mechanism by increasing the fluid pressure, improving the performance of EAM. Guo et al. [14] showed that MRR and surface quality were improved with the increasing fluid pressure during the electrical discharge milling process of graphite on titanium alloy TC4. Li et al. [15] found that the surface machined by SEAM became comparatively flatter with the increasing flushing flow rate, and the thickness of the recast layer decreased. It can be clearly seen that the fluid field plays a critical role in the hydrodynamic arc breaking mechanism, further making a significant impact on surface quality. Gu et al. [11] optimized the fluid field to control the arc plasma more homogeneously, avoiding the deep craters in the center of the machined surface. In fact, the capability to control arc plasma is not sufficient enough when using only one of the above two mechanisms in the actual processing procedure. Therefore, a compound arc breaking mechanism, combining hydrodynamic arc breaking with mechanical motion arc breaking, has been widely adopted as the plasma control mechanism in arc machining, such as BEAM [16].

Multiple sloped surfaces are encountered frequently in 3-axis milling. Some researches have indicated that the relative angle between the electrode and workpiece can have a significant impact on the machining process. Nakano et al. [17] conducted dry electric discharge milling and pointed out that the different angle orientations of the electrodes and workpiece affected the flow velocity of the gas medium, and the gas leak caused a reduction in MRR. Fujiki et al. [18] found that the increase in the tilt angle of the electrode led to a decrease in MRR and an increase in TWR due to the leakage of working fluid. To address the problem, a path planning strategy was proposed based on electrode-workpiece orientation, which avoided leakage of working fluid and enhanced the performance of EDM milling [19]. Undoubtedly, the machining performance is significantly influenced by the relative angle between the electrode and the workpiece. In 3-axis arc milling, the relative inclination angle can be an expanding gap between the tool and the workpiece surfaces. This leads to significant decompression of the working fluid pressure, as depicted in Fig. 1.

Aiming at improving the quality of sloped surfaces in BEAM, this paper aims to investigate the influence of slope angles on surface quality through a series of experiments. Subsequently, an analysis and simulation-based approach is employed to elucidate the reasons behind the deterioration of surface quality. Additionally, the impact of a magnetic field on boosting debris expulsion and plasma control is proved. Finally, experimental validation is conducted to ascertain the efficacy of magnetic field assistance in improving surface quality.

2 Experimental and simulation setup

2.1 Experimental setup

A series of BEAM experiments were conducted using a custom-built BEAM machine to investigate the impact of slope angle on machining outcomes. Inconel 718 bevels with angles of 0°, 20°, 40°, and 70° were selected

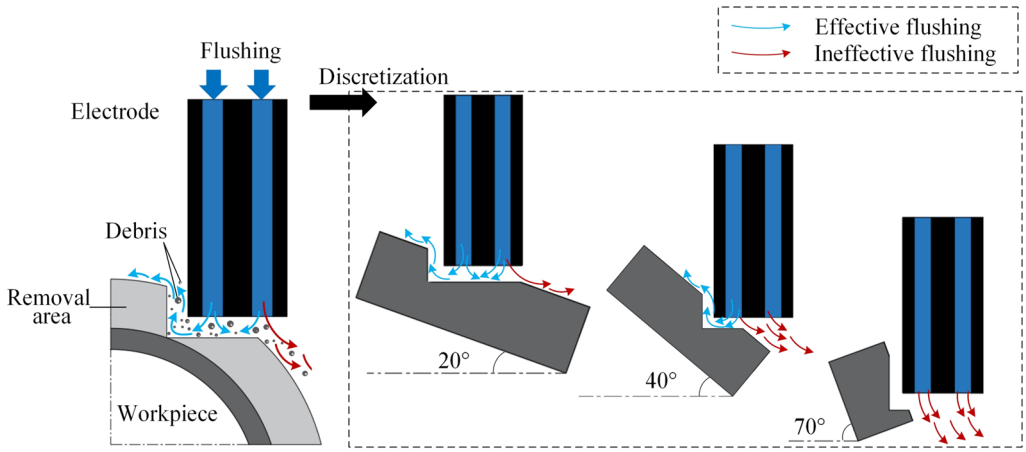

Fig. 1 Schematic of decompression in bevels machining

to perform BEAM machining experiments, as shown in Fig. 2. An adjustable tilting platform determines the position of bevels. The machining feature for all conditions is a single groove with a cutting depth of 3 mm and a length of 40 mm. After machining, the machined surface and its metallograph after grinding and corrosion are observed by a confocal microscope (Keyence VHX-6000), and the drawtube is adjusted to be sideling to fit the morphology of bevels, as shown in Fig. 2c. The machined surface roughness is also measured by that, and the cutoff wavelength of S-filter and L-filter is 80 μm and 20 mm. Additionally, the micromorphology is observed by a scanning electron microscope (Tescan VEGA-3).

Efficiency-first parameters combination is selected to conduct the BEAM experiments, including a current of 650 A, pulse duration of 5.5 ms, and pulse interval of 3 ms. The workpiece is Inconel 718, and the electrode is graphite with multiple flushing holes. Machining experiments adopt the workpiece positive polarity. Other experimental conditions are presented in Table 1. In the case of magnetic-assisted BEAM, a uniform horizontal magnetic field, spanning the entire machining area, was generated using two permanent magnets. Considering that the magnetic field strength is positively related to the control ability of the plasma deflection, the maximum magnetic field available to the device (200 mT) was applied to the bevel machining experiments to better compensate for the loss of the flow field. To analyze the variation in discharge conditions with different angles, the current and voltage waveforms were recorded using an oscilloscope.

Table 1 Experimental conditions

Parameters	Value
Machining angle/(°)	0, 20, 40, 70
Magnetic field strength/mT	0, 200
Open voltage/V	140
Flushing flow/(kg·s^{-1})	0.5
Rotation speed/(r·min^{-1})	1 200

2.2 Simulation model

2.2.1 Simulation model establishing

In BEAM milling, the products are processed by the multi-hole electrode in layer milling. High-speed internal flushing ensures the effect of the hydrodynamic arc breaking mechanism and the debris evacuation, relative to the surface quality. To investigate the influence of slope angles on surface quality, the flow field and particles in the discharge gap are simulated, and the schematic of the simulation model is shown in Fig. 3.

In this research, the diameter and the length of the electrode are 14 mm and 30 mm, respectively. Four flushing holes with a 3 mm diameter are used to realize internal flushing. The rotation speed of the electrode is 1 200 r/min. The discharge gap between the electrode and the workpiece is 0.5 mm, and the flushing fluid thickness is set to the same as that. Meanwhile, considering the electrode wear, the chamfer of the discharge area is set to 0.5 mm.

This simulation is conducted by COMSOL multiphysics and the model is dissected 197 063 grid units. Firstly,

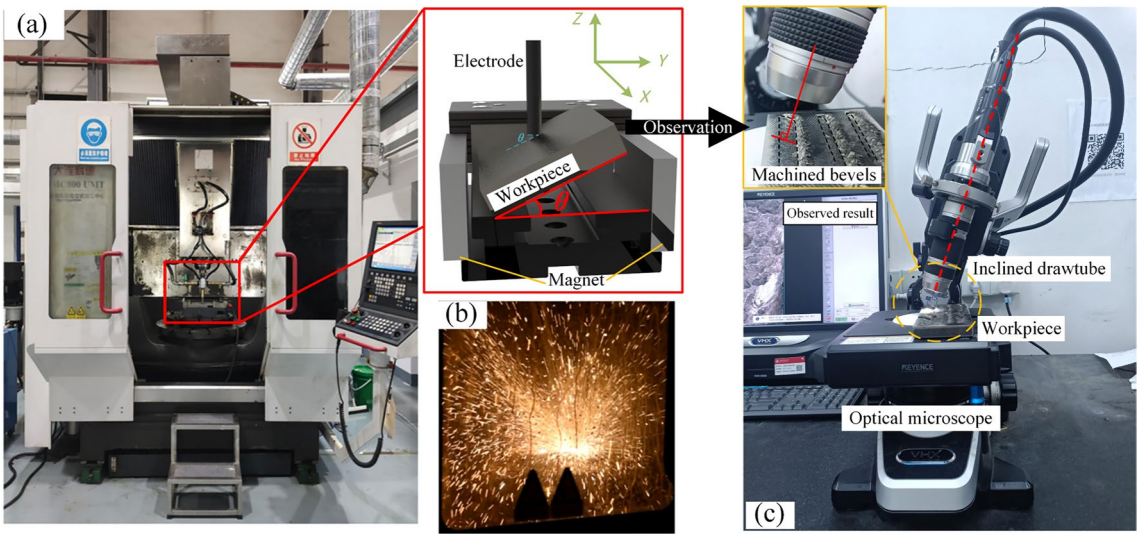

Fig. 2 Experimental setup **a** custom-built BEAM machine and schematic of bevels machining, **b** scene of BEAM in action, **c** observation process of morphology

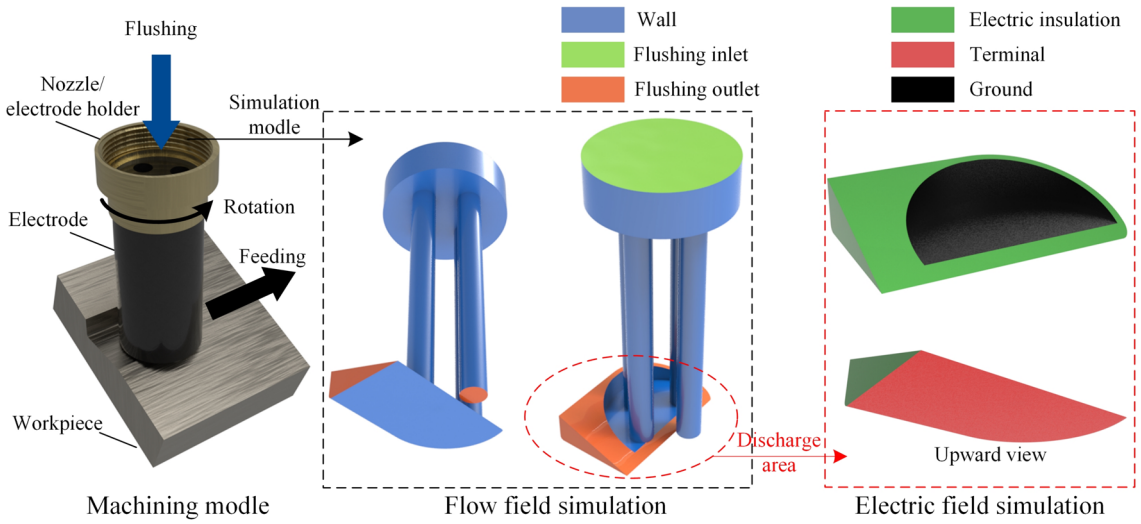

Fig. 3 Simulation model and its boundary conditions

the frozen rotor solver is used to calculate the influence of electrode rotation on the flow field. Based on this, the transient flow field is solved. Then, the movement of the particles under the flushing is solved by the particle tracking module. Moreover, when analyzing the particle motion under magnetic field assisted BEAM (M-BEAM), the electric field of the discharge gap should also be solved to calculate the Lorentz force.

2.2.2 *Simulation assumption*

The flow field in the discharge gap is turbulent and complex, so to simplify the calculation process, the following assumptions are proposed.

(i) The working fluid is considered to be incompressible water at room temperature, regardless of any other added components.
(ii) The effect of bubbles on the flow field is neglected.
(iii) Only the single coupling effect of the flow field and the electric field on the particle are considered.

2.2.3 *Governing equations*

(i) Flow field

The Reynolds number is calculated to be over 4 000, and the flow field is estimated to be turbulent flow. Turbulent flow presents a wide range of flow scales, containing interacting irregular vortices. Its velocity and pressure at any point of the flow field in the flow process vary with time. Therefore, the flow state of the working fluid is described by the k-ε turbulence model, and the transport equation for the turbulent kinetic energy and the turbulent dissipation rate are shown as Eqs. (1)–(2) [20, 21].

$$\rho(\boldsymbol{u}\cdot\nabla)k=\nabla\left[\left(\mu+\frac{\mu_{\mathrm{t}}}{\sigma_k}\right)\nabla k\right]+P_k-\rho\varepsilon, \tag{1}$$

$$\rho(\boldsymbol{u}\cdot\nabla)\varepsilon=\nabla\left[\left(\mu+\frac{\mu_{\mathrm{t}}}{\sigma_\varepsilon}\right)\nabla\varepsilon\right]+C_{\varepsilon1}\frac{\varepsilon}{k}P_k-C_{\varepsilon2}\rho\frac{\varepsilon^2}{k}, \tag{2}$$

where ρ, μ, and $\boldsymbol{u}$ are the density, the dynamic viscosity, and the velocity matrix of the working fluid, respectively; k is the turbulent kinetic energy; ε is the turbulent dissipation rate; σ_k and σ_ε are the Prandtl number of the turbulent kinetic energy and the turbulent dissipation rate, respectively; and $C_{\varepsilon1}$ and $C_{\varepsilon2}$ are the constants. The turbulent viscosity μ_{t} is expressed as Eq. (3). The production term P_k is expressed as Eq. (4) [22].

$$\mu_{\mathrm{t}}=\rho C_\mu\frac{k^2}{\varepsilon}, \tag{3}$$

$$P_k=\mu_{\mathrm{t}}\left[\nabla\boldsymbol{u}:\left(\nabla\boldsymbol{u}+(\nabla\boldsymbol{u})^{\mathrm{T}}\right)\right]. \tag{4}$$

(ii) Particle tracking

The movement of the particles is calculated by Newton's second law, as shown in Eq. (5).

$$m_{\mathrm{p}}\frac{\mathrm{d}v}{\mathrm{d}t}=F_{\mathrm{t}}, \tag{5}$$

where m_p is the particle mass; v is the particle velocity; t is time; F_t is the external force, and in this research, the external forces are fluid drag force and Lorentz force.

(iii) Electric field

The magnetic field impacts the trajectory of charged particles by the Lorentz force, which is calculated by

$$F_m = qv \times B, \tag{6}$$

where q is the particle charge, which is calculated through the current density of the electric field. The electric field of the discharge gap is calculated by Ohm's law, as shown in Eqs. (7) and (8). B is the magnetic strength.

$$J = \sigma E, \tag{7}$$

$$E = -\nabla V, \tag{8}$$

where J is the current density; σ is the conductivity; E is the electric field; and V is the electric potential.

2.2.4 Boundary conditions

(i) Flow field

The solution domain for the flow field simulation is the fluid inside the electrode and the discharge zone. It involves three kinds of boundaries, including flushing inlet, flushing outlet, and wall boundary. The flushing inlet is the top surface of the nozzle where the working fluid flushes into the electrode and it is set to mass flow as 0.5 kg/s, which is acquired from the flow meter in the actual machining process. The flushing outlet is the area around the discharge area and its reference pressure is set to 0 MPa [16]. Other boundaries are set to the wall boundary condition with no slip. Considering the effect of surface roughness on the fluid flow, the surface roughness of the wall boundaries is set in the simulation model. Specifically, the roughness of the electrode wall and the workpiece wall is set to 6.4 μm and the measured value, respectively.

(ii) Electric field

The solution domain for the electric field is the discharge zone. It also involves three kinds of boundaries, including terminal boundary, ground boundary, and electric insulation boundary. In the actual machining process, the workpiece and electrode are connected to the positive and negative pole of the power supply which is output at a constant current of 650 A. Therefore, the fluid boundary in contact with the workpiece surface is set to the terminal of 650 A; the fluid boundary in contact with the electrode is set to ground; and the other boundaries are set to electric insulation.

(iii) Particle tracking

The solution domain for the particle tracking is the discharge zone. The particle inlet is the front area of the discharge zone, where the discharge and material removal mainly occur. Considering that the debris is carried away by flushing, the outlet is the same as the flushing outlet, while others are set to diffuse scattering. The debris produced by BEAM are mostly nearly spherical particles with an average diameter of 100 μm [16]. According to the particle volume and MRR, the particle number produced during a pulse period is 2 520. Neglecting the different particle production rates at different locations, the particle release is assumed to be the same homogeneous rate for every 0.5 ms 210 until the pulse duration ends [23]. Additionally, the charge of particles is calculated according its position and volume.

3 Impact of slope angles on the surface quality

3.1 Experimental results of bevel machining with BEAM

Figure 4 depicts the surface topography obtained from BEAM under different machining angles. In the case of planar machining, a relatively uniform surface is achieved, exhibiting fewer anomalous discharge traces and deep craters. However, as the machining angle increases, distinct changes in surface characteristics are observed. Specifically, on the 20° bevel surface, some deep craters become apparent. On the 40° bevel surface, plowed grooves along the electrode rotation direction start to emerge. The surface quality is most compromised on the surface of the 70° bevel, exhibiting numerous deep grooves and over-burned traces. These observations suggest that as the machining angle increases, the arc plasma becomes increasingly difficult to break or even deflect due to losing the control ability. Consequently, the high energy is concentrated on a narrow localized area, leading to surface over-burning. In addition, the scale of the four images is different. On the one hand, as shown in Fig. 1, as the machining angle increases, the width of the machining zone becomes shorter for the same cut depth. The different scales of the images are attempted to represent the difference in the size of the machining area. On the other hand, the increased machining angle causes greater undulation of the machined surface, which makes it difficult for the microscope to focus on a large scale. Therefore, the observable area is reduced accordingly.

Based on voltage and current waveforms, the influence of the slope angle on the discharge state is further revealed.

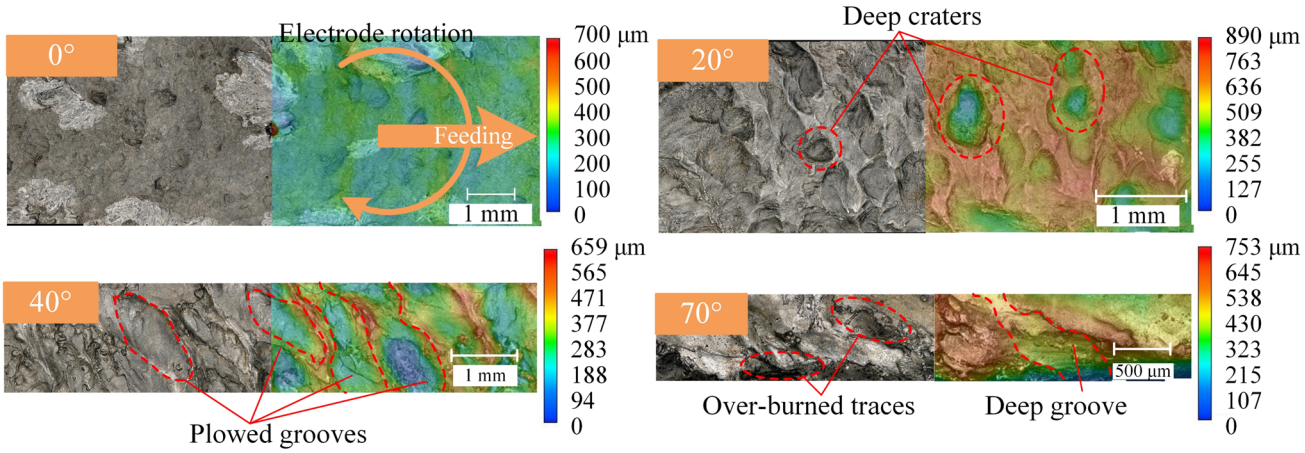

Fig. 4 Surface topography with different machining angles

In addition to open circuit, four distinct discharge types can be identified in BEAM: short circuit, stable arc, disturbed arc, and broken arc. The voltage and current schematics of these four discharge types are shown in Fig. 5a. Short circuit occurs when the positive and negative poles have direct contact, causing a very low voltage and high current. Stable arc is manifested by the voltage dropping from the open voltage value to the holding voltage value after the breakdown, while the current increases to and maintains the setting value simultaneously, lasting a full pulse duration. In BEAM, both short circuit and stable arc are considered detrimental and undesirable, because the thermal energy from the two discharges are concentrated on the workpiece surface. In particular, it is crucial to avoid short circuits because its extremely high energy may destroy the workpiece. By employing arc breaking methods, the arc plasma can be disturbed or even broken. When the arc plasma is disturbed, it becomes unstable and the waveform fluctuates, resulting in a rise in voltage and a fall in current. Further, when the disturbance aggravates, the plasma channel is hard to maintain and broken, which characterizes the voltage and the current return to the open voltage value and zero, respectively. Effective arc disturbance facilitates the timely dispersal of arc plasma heat, thereby protecting the surface from over-burning. Consequently, the presence of disturbed arc and broken arc is desirable in BEAM and contributes to the improvement of surface quality.

Through the collected waveforms, the proportion of discharge types at different machining angles is counted, as shown in Fig. 5b. When the angle between the electrode and workpiece surfaces is 0° and 20°, the desirable discharge accounts for 76.67% and 74.80%, respectively, with the short circuit being rarely detected. This shows rarely stable arc exists and results in a relatively flat surface. However, as

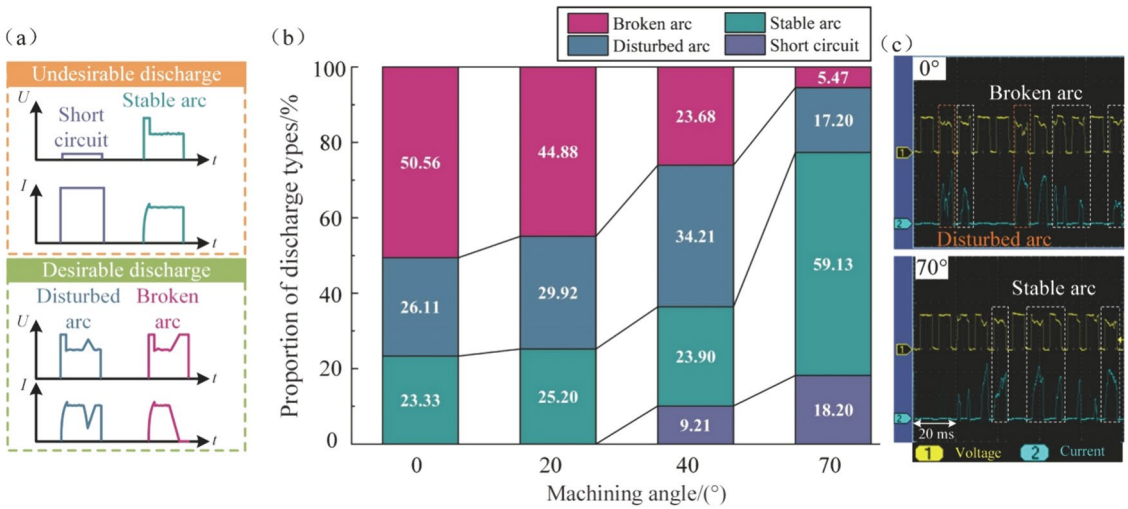

Fig. 5 Schematic of typical discharge waveforms and their proportions

the angle increases to 40°, short circuit starts to appear, and the proportion of desirable arcs decreases to 57.89%. Corresponding to the machined surface topography, it indicates that the effect of hydrodynamic force weakens and the mechanical motion arc breaking dominates. The situation worsens at 70°, where the proportion of desirable discharges drops to only 22.67%, while the ratios of stable arc and short circuits increase rapidly to 59.13% and 18.20%, respectively, causing the worst and over burned surface. It is evident that as the slope angle increases, the percentage of undesirable discharges significantly rises, indicating a substantial reduction of plasma control capability. Especially, as Fig. 5c shows, the discharge types at 0° are dominated by broken arc and disturbed arc, while at 70° stable arc dominates.

3.2 Simulation of gap flow field and debris expelling in BEAM

Since BEAM employs the compound arc breaking mechanism to regulate the behavior of the arc plasma and the mechanical motion generated by electrode rotation remains insensitive to slope angles, the reduction of plasma control effectiveness is primarily attributed to the weakening of the hydrodynamic arc breaking effect. To investigate the influences of slope angles on hydrodynamic force, simulations were conducted to analyze the flow field under different machining angles, as illustrated in Fig. 6. When the slope angle is 70°, no flushing enters the discharge area. Based on this, if the angle continues to increase, the flushing still does not enter the discharge zone. Therefore, the results with 70° can represent the case where no flushing enters the discharge gap.

Previous studies have suggested that maintaining a flushing velocity over 10.5 m/s can effectively control the arc plasma and is crucial for achieving a smooth surface [24]. Consequently, regions where the flushing velocity falls within this range are considered effective flushing areas. The flow field simulation on the machined surface is analyzed, and the ratio of the effective flushing area to the total discharge area and the maximum flushing velocity are statistically calculated, as shown in Fig. 7. In the case of planar machining, the ratio of the effective flushing area exceeds 90%, indicating powerful hydrodynamic force and effective plasma control. For 20° bevel machining, the effective flushing area drops below 80%, resulting in the stabilization of stable arc and the appearance of deep craters. Even worse, as the machining angle increases to 40°, over half of the machining area experiences ineffective flushing. Consequently, mechanical motion arc machining becomes predominant, leading to the formation of deep grooves along the direction of electrode rotation. This is because arc plasma keeps burning without extinction under the mechanical motion arc breaking mechanism [25]. Notably, at a machining angle of 70°, almost no direct flushing enters the discharge area, resulting in the ratio of broken arc being only 5.47%.

The weakening of the flushing effect in large machining angles is correlative to the reduction of the working fluid flow into the discharge gap. As shown in Fig. 6, when the machining angle increases, the discharge area becomes smaller and hard to provide the same back pressure to all the flushing holes, causing the flushing holes gradually exposed to the non-discharge area with low resistance. The exposed flushing holes make the work fluid incline to flow directly out of the non-discharge area rather than into the discharge area. Therefore, all the flushing enters the discharge area in planar machining, but with the increasing slope angles, less working fluid entering the discharge gap leads to less effective flushing. Until the machining angle is 70°, all the working fluid flows to the non-discharge area and nearly loses the ability to control the arc plasma. Meanwhile, it is easy to observe that the center of the discharge area exists

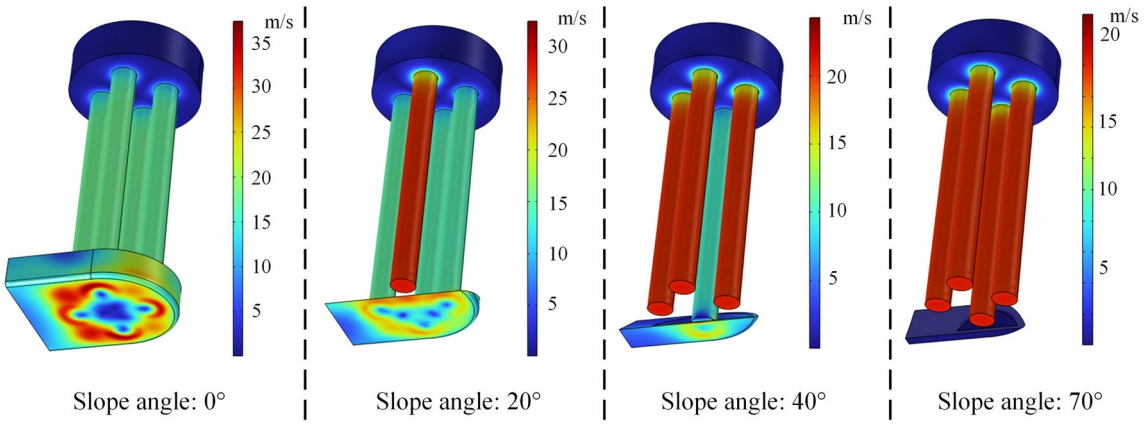

Fig. 6 Flow field simulation under different machining angles

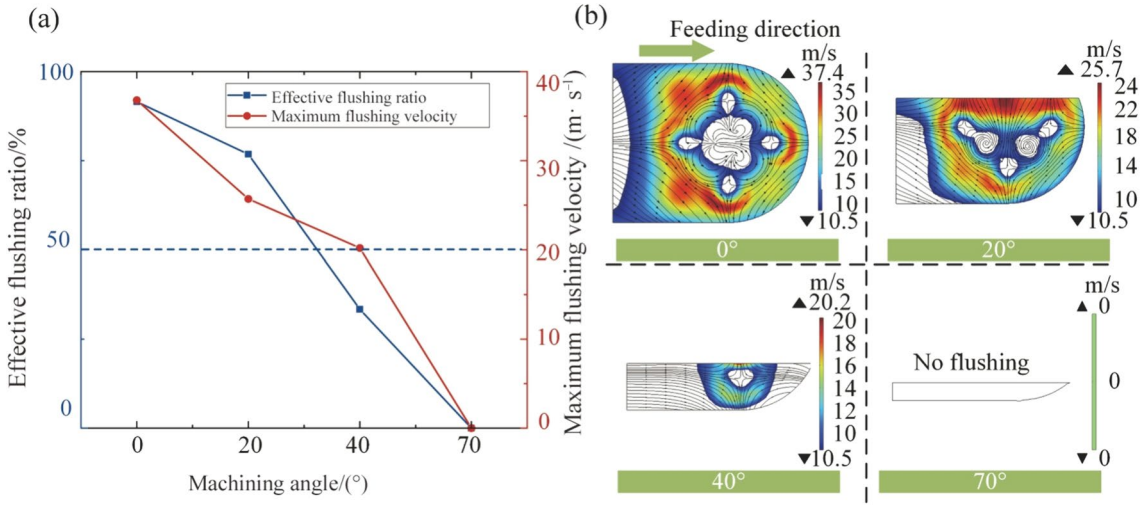

Fig. 7 **a** Effective flushing ratio and maximum flushing velocity, **b** simulation results of the effective flow field

zone that does not meet the criteria for effective flushing. This causes the stable arc to be prone to form in the discharge area center and damages the workpiece surface, which is consistent with research in Ref. [11]. Additionally, the large machining angle results in a significant loss of flushing velocity, thereby limiting arc plasma deflection and impeding deflection response.

In addition to its impact on plasma control, flushing also plays a crucial role in debris evacuation, which significantly affects surface quality. To evaluate the debris expelling effects at different machining angles, particle tracking simulations were conducted. During the pulse duration, the high pressure of the plasma hinders the penetration of flushing, resulting in a gradual increase in the number of particles. On the contrary, in the pulse interval, the particle number decreases rapidly due to the effective flushing into the molten pool, as shown in Fig. 8. As shown in Fig. 4, the flow field between electrodes becomes smaller as the machining angle increases. Since it is difficult for fluid to enter the plasma during the pulse duration, the particles move only by the initial velocity of the explosion, which is independent of the angle. The smaller range of discharge gap makes it relatively easy for the debris to leave, so the particle accumulation rate at a large angle is lower during the pulse.

However, during the pulse interval, as the machining angle increases, the effective flushing effect is significantly weak, hence it is difficult to carry the particles away and make them accumulate [26]. That may lead to a short circuit

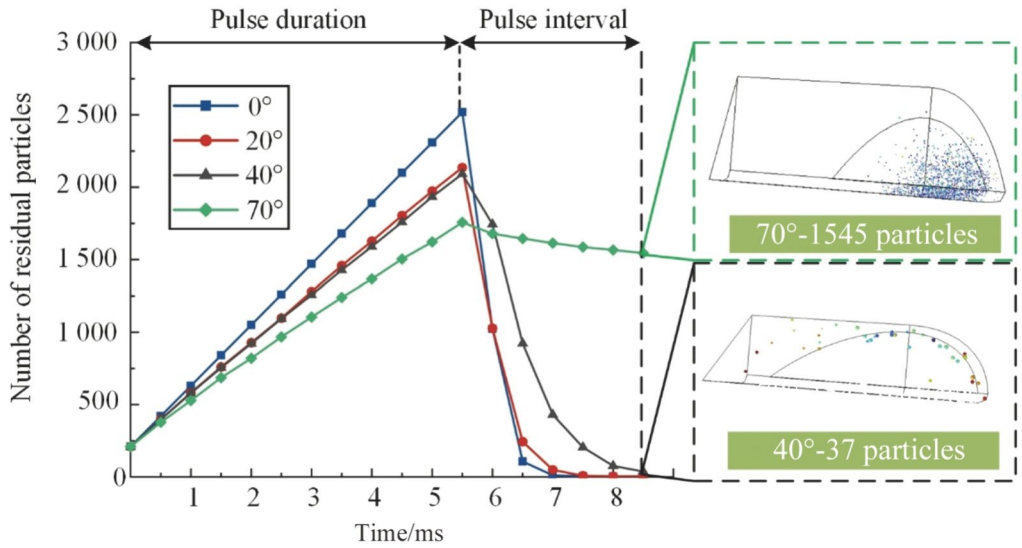

Fig. 8 Number of residual particles in the discharge gap

or secondary discharge in the next pulse, causing damage to the machined area. When the machining angle is below 20°, no particles are residual in the discharge gap after a complete discharge period. Consequently, no short circuit occurs in this case. However, at a 40° machining angle, short circuit and the deep craters produced by secondary discharge begin to appear because the debris is starting to accumulate. Particularly, with a machining angle of 70°, the reduction in residual particle number is not evident during the pulse interval. The accumulation of a significant number of particles leads to a sharp increase in the proportion of short circuits, also accelerating the deterioration of the surface quality.

Therefore, the impact of slope angles on the surface quality can be explained by the increasing machining angle making less working fluid flush into the discharge gap and resulting in a lower effective flushing ratio. The decrease in effective flushing leads to a weakening in plasma control, increasing the occurrence of undesirable discharges. Additionally, weakened flushing causes the accumulation of residual particles and further exacerbates the deterioration of the machined surface. These factors highlight the importance of plasma control and maintain effective debris expelling to achieve high-quality surfaces in sloped surface machining. Exploring alternative energy fields to compensate for the fluid flushing and thus enhance arc plasma control and debris removal becomes a promising avenue.

4 Enhancement of surface quality with magnetic field

4.1 Principle of magnetic field assisted BEAM (M-BEAM)

The addition of a magnetic field in BEAM has the potential to enhance machining performance due to the electromagnetic force that can be exerted on moving charged objects, including electrons, ions, and generated debris. The schematic diagram of M-BEAM is presented in Fig. 9. The magnetic field plays a dual role in M-BEAM. Firstly, it promotes the directional motion of the charged particles composing the arc plasma and thereby deflects the arc at an earlier stage and a longer distance [27]. By combining the electromagnetic force and the hydrodynamic force, the plasma control effect is strengthened. Secondly, the magnetic field drives the discharged molten metal during the pulse duration. Consequently, most molten metal is propelled by the magnetic field during the pulse duration and the residual part is subsequently evacuated through high-speed flushing. This sequential interaction of the magnetic field and flow field allows for effective impact on both the arc plasma and debris, without any conflict. Therefore, the magnetic field is selected to serve as a complement to compensate for the loss of flushing efficiency. This will be further illustrated through an analysis of discharge conditions and simulations of debris evacuation.

4.2 Behavior of arc plasma and debris in M-BEAM

In the previous study, it was found magnetic field deflected the arc plasma timelier than the other two arc breaking mechanisms because it directly acted on the charged particles making up the plasma. Larger magnetic field strength results in longer arc plasma deflection and higher debris movement speed [27]. The plasma behavior of the discharge in the air is captured by a high-speed camera under a 200 mT magnetic field, as shown in Fig. 10. The arc plasma deflects at 0.35 ms after breakdown and the deflection is over 10 mm at 3.0 ms. The arc plasma movement speeds are calculated by the post-processing software PCC CD image of a high-speed camera, which are 35.16 m/s, 55.32 m/s, and 78.12 m/s at 0.5 ms, 0.75 ms, and 1.0 ms after breakdown, respectively. The arc plasma moves with nearly uniform acceleration because of the constant electromagnetic force. Meanwhile, the arc plasma movement speed at 1.0 ms is aready much higher than the maximum flushing speed (37.4 m/s from the simulation). It indicates that the arc plasma is powerfully controlled even if only driven by the magnetic field, which significantly disperses the thermal effect of the plasma and would protect the workpiece from overburning. In addition, a mass of molten metal is significantly observed to be expelled from the molten pool, favoring the reduction of residual debris in the discharge gap.

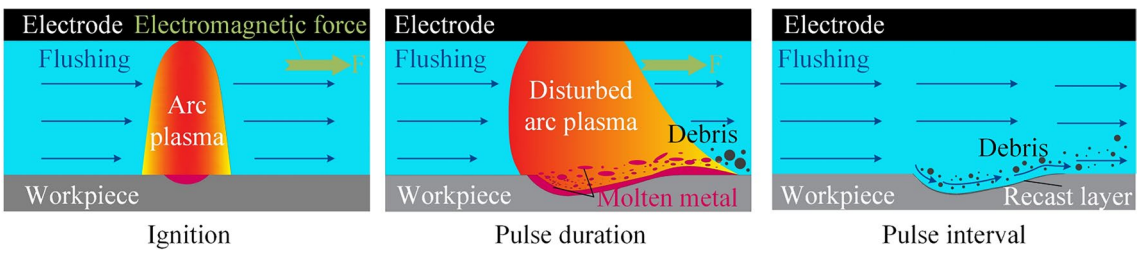

Fig. 9 Schematic of magnetic field assisted BEAM

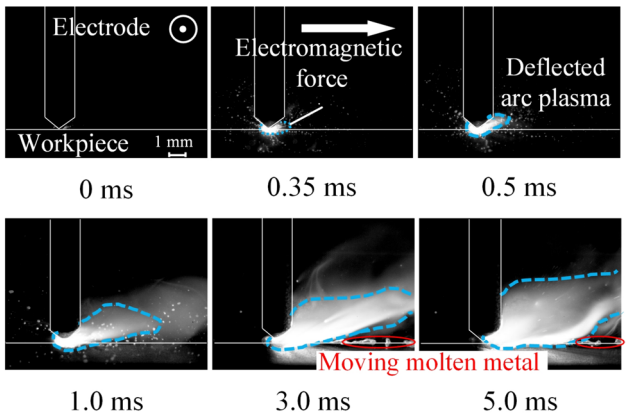

Fig. 10 Control effect of magnetic field on arc plasma and molten metal

To investigate the effectiveness of the magnetic field in debris evacuation, a particle tracking simulation model considering the electromagnetic force was developed. The results, displayed in Fig. 11, demonstrate the impact of the magnetic field on the number of residual particles. The hydrodynamic force is an external and passive force for arc plasma and molten metal, while the electromagnetic force is internal and active. Thus, different from the flow field which struggles to penetrate the high-pressure plasma and effectively carry away debris during the pulse duration, the magnetic field actively drives the charged debris away from the machining gap. When the machining angle is large, the magnetic field still promotes the debris expelling despite the loss of effective flushing. As a result, the accumulation rate of particles decreases significantly when the magnetic field is applied. Specifically, for machining angles of 20°, 40°, and 70°, the accumulation rates decrease from 350.18, 342.18, and 281.27 per microsecond to 162.73, 174.73, and 126.18 per microsecond, respectively. This reduction in debris accumulation leads to nearly half the number of residual particles compared to traditional BEAM at the end of the pulse duration. Further, during the pulse interval, the presence of the magnetic field results in a lower number of particles in the discharge gap compared to situations without a magnetic field, even when flushing is weakened due to large slope angles. M-BEAM facilitates a continuous process in which debris is expelled throughout the entire discharge pulse. The number of residual particles under M-BEAM is only 51.35% and 40.78% of that observed on surfaces with a 40° and 70° machining angle, respectively, compared to traditional BEAM. Therefore, the effect of the magnetic field on arc plasma control and debris expelling would improve the discharge condition, which was also proved by the experiments in Refs. [28, 29].

4.3 Experimental results of bevels machining with M-BEAM

To investigate the influence of the magnetic field on the discharge condition, the waveforms in M-BEAM were analyzed and the statistical distribution of each discharge type was presented in Fig. 12. In the case of planar machining, the proportion of desirable discharge increased by 8.81% compared to traditional BEAM. Moreover, the magnetic field improves the desirable discharge ratio by more than 10% for machining bevels at all angles. When the slope angle is below 40°, the desirable discharge accounts for more than 70% of the total discharges. This demonstrates the effectiveness of the magnetic field in promoting desirable discharges.

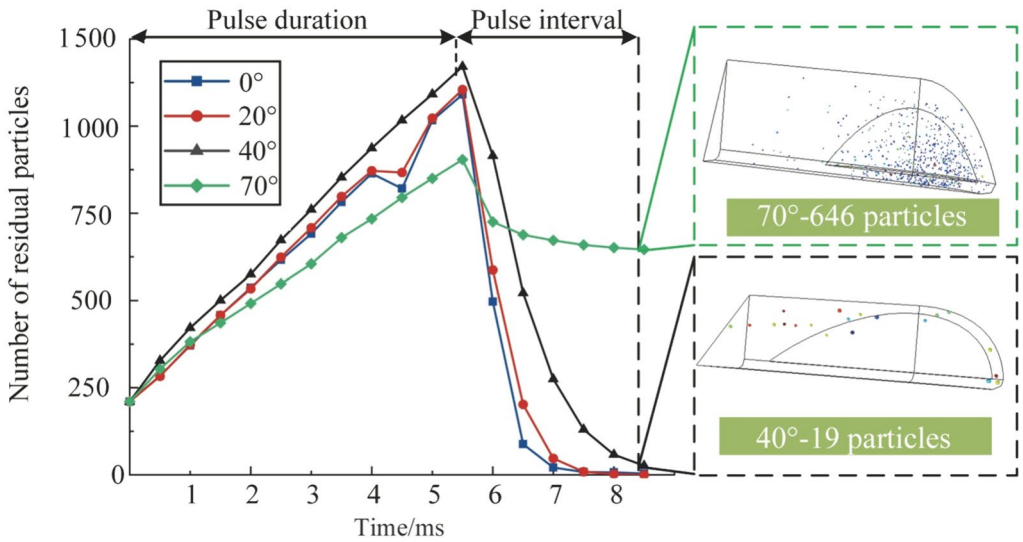

Fig. 11 Number of residual particles in the discharge gap in M-BEAM

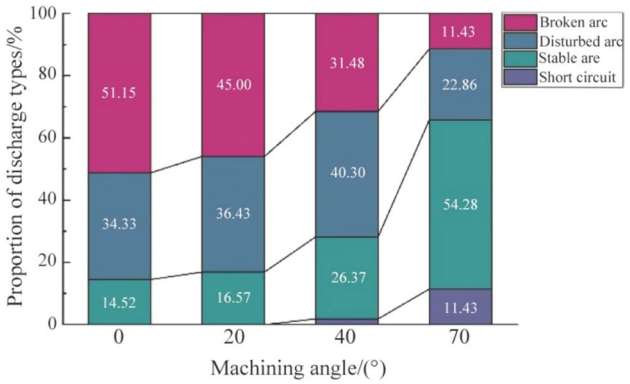

Fig. 12 Proportion of different discharge types in M-BEAM

Furthermore, even in situations where the flow field cannot effectively flush into the discharge gap, the magnetic field still contributes to a desirable discharge rate of 34.29%. This indicates that the magnetic field plays a crucial role in improving discharge characteristics, even when flushing is hindered. The increase in desirable discharge has several positive effects on the machining process. Firstly, it leads to a more efficient dispersion of the heat generated by the arc plasma. This results in shallower and larger craters, ultimately leading to a flatter machined surface. Additionally, the reduction in residual debris decreases the probability of short circuits occurring. With a machining angle of 40°, short circuits are nearly non-existent, and their occurrence probability decreases to 11.43% in 70° bevel machining. This reduction in short circuit probability helps protect the machined surface from damage. However, the improvement of desirable discharge decreases with increasing machining angle. From 20° to 70°, the increase in the proportion of desirable discharge reduces from 16.63% to 11.62%. This indicates the indispensable of the flow field, and the magnetic field is an effective complement to it rather than a substitute.

The introduction of M-BEAM has led to a notable improvement in the quality of the machined surfaces, as shown in Fig. 13. For machining angles lower than 40°, the machined surfaces appear relatively smooth due to the sustained high desirable discharge rate. In comparison to traditional BEAM, the surface with a 20° angle no longer exhibits large and deep craters, which means that the arc plasma is timely deflected and broken. Similarly, on the 40° angle bevels, the long and deep ravines are wider and shallower, indicating that the magnetic field improves the control effect of arc plasma and the mechanical motion arc breaking mechanism does not dominate. Furthermore, the undulation on the 70° angle surface becomes smaller, resulting in a more uniform appearance, demonstrating the benefit of reducing the short circuit. The positive impact of M-BEAM on surface quality is further supported by the reduction in surface roughness (S_a) observed across all machined bevels. With the assistance of the magnetic field, the surface roughness is reduced by more than 15 μm compared to traditional BEAM when machining bevels. However, when the machining angle is 70°, even though the magnetic field improves discharge condition, the surface roughness is still unsatisfactory, reaching over 100 μm. It suggests that the bevels with

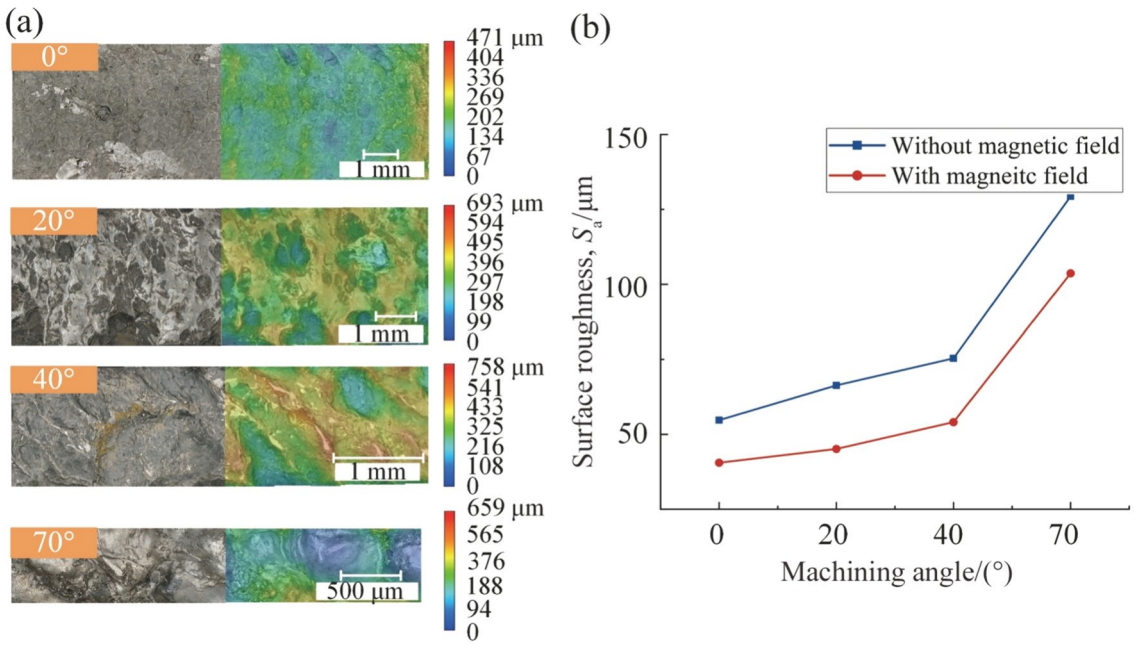

Fig. 13 **a** Topography of machined surface in M-BEAM, **b** comparison of surface roughness with and without magnetic field

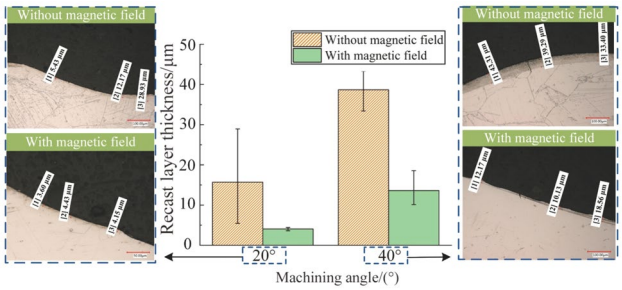

Fig. 14 Metallographic photographs of machined surfaces

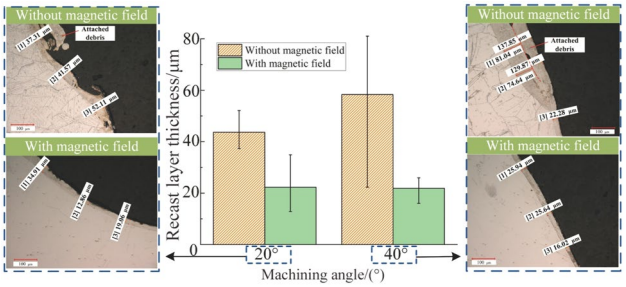

Fig. 15 Metallographic photographs of side walls

an angle over 40° should be avoided when designing the machining trajectories.

Except for the planar and 70° beveled surface, the micro surface quality of bevels with 20° and 40° angles are further analyzed. The metallographic analysis of the cross-sectional surface and the recast layer thickness is presented in Fig. 14. When machining bevels with traditional BEAM, the loss of effective flushing hinders the expulsion of molten metal, resulting in a thick and detrimental recast layer. Meanwhile, a thick recast layer frequently accompanies cracks, mitigating the connection with subsequent finishing machining processes. In contrast, the magnetic field in M-BEAM disperses the arc's energy and pushes the molten metal away, leading to a thinner recast layer. Compared with traditional BEAM, the recast layer thickness under M-BEAM is reduced by 74.12% and 64.78% for 20°and 40° bevels, respectively.

Furthermore, the metallography of the side wall is observed in Fig. 15. Compared with Fig. 14, the recast layer of the side wall is thicker than that of the machined surface for all the same conditions, due to the weaker flushing effect in the side discharge gap. The insufficient flow field hardly flushes away the molten metal and debris, causing the side wall with thick recast layer and attached debris when the magnetic field is not applied. The effect of the magnetic field on reducing the recast layer is still evident, keeping it around 20 μm at both 20° and 40° bevels.

The surface micromorphology is examined using scanning electron microscopy (SEM), as shown in Fig. 16. In traditional BEAM, undesirable phenomena such as molten metal accumulation, debris attachment, and micro cracks are observed on the machined surface and become more severe as the slope angle increases. This also reflects the molten metal is expelled insufficiently with the gradual loss of flow field. Conversely, in M-BEAM, the surface is smoother and the occurrence of these undesirable phenomena is noticeably reduced. This can be attributed to the more effective expulsion of molten metal facilitated by the magnetic field.

5 Conclusions

In this research, the influence of slope angle on surface quality is studied through the simulation of flow field and particle tracking, pointing out that the deterioration of surface quality with increasing machining angle is due to the gradual loss of effective scouring. After applying the magnetic field, both the arc plasma control and debris expelling are enhanced, improving the discharge condition and thus achieving a better surface. Based on the results

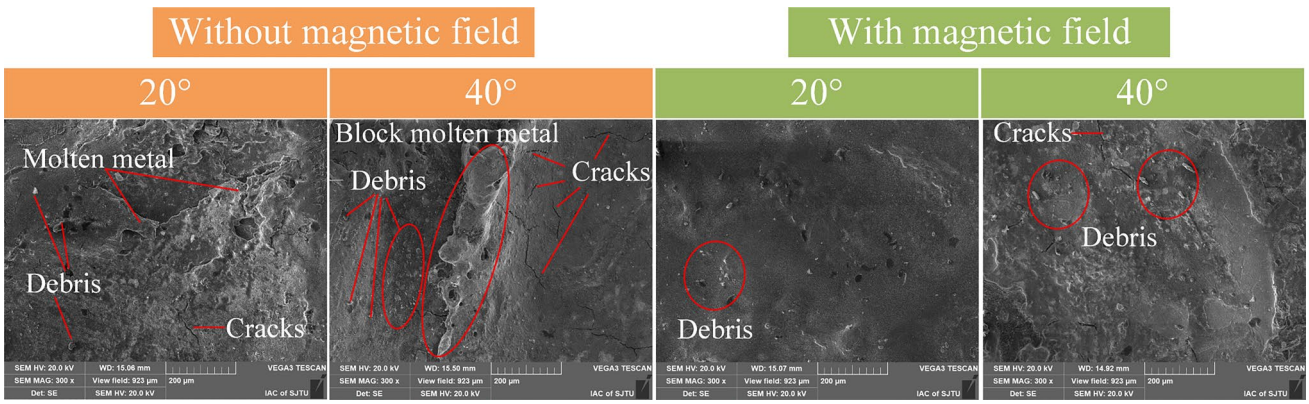

Fig. 16 Machined surfaces observed by SEM

obtained from experiments and simulations, the following conclusions can be drawn.

(i) The decrease in effective flushing, leading to a weakening of arc plasma control and the accumulation of residual particles, and then resulting in increasing undesirable discharge ratio, is identified as the main reason for the decrease in surface quality when machining sloped surfaces.

(ii) The application of a magnetic field in M-BEAM effectively controls the arc plasma and reduces residual particles accumulation by more than 50% compared to traditional BEAM, increasing the proportion of desirable discharge by more than 10% for all bevels and significantly reducing the proportion of short circuit.

(iii) The sloped surface quality indicated that M-BEAM could offer a more uniform and smoother surface with smaller surface roughness, thinner recast layer, and less quantity of debris and microcracks. To acquire a satisfactory surface, the machining angle should be lower than 40° when designing the machining trajectory.

Acknowledgements Part of this study was supported by the National Natural Science Foundation of China (Grant No. 51975371). Besides, the authors also acknowledge the SEM and EBSD tests developed at the Instrumental Analysis Center of SJTU.

References

1. Zhang B, Zeng Y, Pang X et al (2022) Feasibility analysis and process characteristics of selective laser ablation assisted milling Inconel 718. Adv Manuf 10(4):495–519
2. Chen J, Gu L, Zhao W et al (2020) Modeling of flow and debris ejection in blasting erosion arc machining in end milling mode. Adv Manuf 8:508–518
3. Meshcheriakov G, Nosulenko V, Meshcheriakov N et al (1988) Physical and technological control of arc dimensional machining. CIRP Ann Manuf Tech 37(1):209–212
4. Wei B, Trimmer A, Luo Y et al (2010) Advancement in high-speed electroerosion processes for machining tough metals. In: Proceedings of the 16th international symposium on electromachining, pp 193–196, Shanghai
5. Zhao W, Gu L, Xu H et al (2013) A novel high efficiency electrical erosion process—blasting erosion arc machining. Procedia CIRP 6:621–625
6. Krotz H, Roth R, Wegener K (2013) Experimental investigation and simulation of heat flux into metallic surfaces due to single discharges in micro-electrochemical arc machining (micro-ECAM). Int J Adv Manuf Technol 68:1267–1275
7. Wang F, Liu Y, Zhang Y et al (2014) Compound machining of titanium alloy by super high speed EDM milling and arc machining. J Mater Process Technol 214(3):531–538
8. Wu X, Liu Y, Zhang P et al (2023) Electrical discharge and arc milling with automatic tracking of optimal flushing direction: a novel high- efficiency compound machining method. Chin J Aeronaut 37:351–364
9. Xu H, Gu L, Chen J et al (2015) Machining characteristics of nickel-based alloy with positive polarity blasting erosion arc machining. Int J Adv Manuf Technol 79:937–947
10. Liu Z, Liu K, Dai X et al (2022) Milling performance of Inconel 718 based on DC short electric arc machining with graphite and W-Ag electrode materials. Int J Adv Manuf Technol 122(5):2253–2265
11. Gu L, He G, Li K et al (2022) Improving surface quality in BEAM with optimized electrode. CIRP Ann Manuf Technol 71:165–168
12. Kou Z, Han F, Wang G (2019) Research on machining Ti6Al4V by high-speed electric arc milling with breaking arcs via mechanical-hydrodynamic coupling forces. J Mater Process Technol 271:499–509
13. Gu L, Zhang F, Zhao W et al (2016) Investigation of hydrodynamic arc breaking mechanism in blasting erosion arc machining. CIRP Ann Manuf Technol 65(1):233–236
14. Guo C, Wei D, Di S (2016) Improving energy utilization efficiency of electrical discharge milling in titanium alloys machining. J Cent South Univ 23:2550–2557
15. Li X, Li Z, Wu T et al (2023) Experimental research on short electric arc milling machining based on the mechanical-fluid coupling effect. Proc Inst Mech Eng Part B-J Eng Manuf 237(9):1353–1363
16. He G, Gu L, Zhu Y et al (2022) Electrical arc contour cutting based on a compound arc breaking mechanism. Adv Manuf 10:583–595
17. Nakano S, Shibayama T, Kunieda M et al (2005) Curved surface machining by dry EDM using 5-axis machine. In: Proceedings of JSPE semestrial meeting, pp 838–838, Tokyo
18. Fujiki M, Ni J, Shih AJ (2009) Investigation of the effects of electrode orientation and fluid flow rate in near-dry EDM milling. Int J Mach Tool Manuf 49(10):749–758
19. Fujiki M, Ni J, Shih AJ (2011) Tool path planning for near-dry EDM milling with lead angle on curved surfaces. J Manuf Sci E-T Asme 133(5):051005. https://doi.org/10.1115/1.4004865
20. Guo C, Sun S, Di S et al (2021) Experimental and simulation study of the ED-milling flow field to improve its machining performance. Int J Adv Manuf Technol 113:2513–2522
21. Guo X, Tan L, Xie Z et al (2024) Simulation and experimentation of renewable dielectric gap flow fields in EDM. Int J Adv Manuf Technol 130(3):1935–1948
22. Wang X, Guo H, Wu G et al (2022) Hydrodynamic arc moving mechanism in EDM of polycrystalline diamond. Mater Manuf Process 37(14):1652–1663
23. Lin L, Liu Y, Xue W et al (2023) Improving the machined surface in electrochemical mill-grinding by particle tracking fluid simulation and experimental research. Phys Fluids 35(12):123319. https://doi.org/10.1063/5.0176244
24. Gu L, Farhadi A, Zhu Y et al (2020) A novel tool design procedure for arc sweep machining technology. Mater Manuf Process 35(1):113–121
25. Kou Z, Han F (2018) Machining characteristics and removal mechanisms of moving electric arcs in high-speed EDM milling. J Manuf Process 32:676–684
26. Jiang Y, Kong L, Ping X et al (2021) Utilizing a porous-electrode for the flushing fluid in electrical discharge machining. J Manuf Process 62:248–256
27. Li K, Wang X, Jiang L et al (2024) Study of arc behavior and machining effects of the novel magnetic field assisted blasting erosion arc machining method. J Mater Process Tech 323:118227. https://doi.org/10.1016/j.jmatprotec.2023.118227
28. Lin Y, Lee H (2008) Machining characteristics of magnetic force-assisted EDM. Int J Mach Tools Manuf 48:1179–1186

29. Lin Y, Chen Y, Wang D et al (2009) Optimization of machining parameters in magnetic force assisted EDM based on taguchi method. J Mater Process Technol 209:3374–3383

Lin Gu received his Ph.D. degree in Engineering from Harbin Institute of Technology. He is currently an associate professor in the State Key Laboratory of Mechanical System and Vibration, School of Mechanical Engineering, Shanghai Jiao Tong University, China. His research interests include advanced manufacturing technology for difficult-to-cut materials, such as EDM, arc discharge machining, and compound machining.

Ke-Lin Li is currently pursuing a doctoral degree at the State Key Laboratory of Mechanical System and Vibration, School of Mechanical Engineering, Shanghai Jiao Tong University, China. His research interests include the technical and equipment of electrical arc machining (EAM) and magnetic field assisted machining.

Xiao-Ka Wang is a PH.D. candidate at the State Key Laboratory of Mechanical System and Vibration, School of Mechanical Engineering, Shanghai Jiao Tong University, China. His current research interests include blasting erosion arc machining (BEAM) and processing of ceramic material.

Guo-Jian He is a Ph.D. candidate at the State Key Laboratory of Mechanical System and Vibration, School of Mechanical Engineering, Shanghai Jiao Tong University, China. His research interests include the technical and equipment of electrical arc machining (EAM) and micro electrical discharge machining (micro-EDM).